A study of the Al–Co–Pt alloy system

B. Grushko •

ERC-1, Forschungszentrum Jülich, 52425 Jülich, Germany

Abstract

Phase equilibria in the Al-rich part of Al–Co–Pt are studied at 1100 °C below 35 at.% Pt, at 850 °C below 25 at.% Pt and at 700 °C above 75 at.% Al. The maximal ternary extensions of Al_9Co_2 and m-$Al_{13}Co_4$ were found to have achieved ~4 and ~2 at.% Pt, respectively, those of Al_4Pt and ξ_{Pt} ~8 and 3.5 at.% Co, respectively. The ternary extension of Al_2Pt was found to propagate up to at least $Al_{57}Co_{16}Pt_{27}$. The formation of four ternary phases, designated χ, ε, D and æ, was revealed. The χ-phase (*P*31*c*, *a* = 1.21617 nm, *c* = 2.7115 nm) was revealed between ~$Al_{76.5}Co_{11}Pt_{12.5}$ and $Al_{75}Co_4Pt_{21}$. The ε-phase (ε_6-type, *Pnma, a* = 2.3116 nm, *b* = 1.6363 nm, *c* = 1.2150 nm) was revealed between ~$Al_{75}Co_{17}Pt_8$ and $Al_{72}Co_7Pt_{21}$. The D-phase of the D_2-type (~0.8 nm periodicity in the specific direction perpendicular to quasiperiodic planes) is formed at elevated temperatures in a small compositional region around $Al_{73.4}Co_{23.3}Pt_{3.3}$. The structure of an æ-phase forming around ~$Al_{71}Co_{20}Pt_9$ and exhibiting a complex powder XRD pattern was not specified.

Keywords: Transition metal alloys and compounds; Phase diagrams.

1. Introduction

While the boundary binary Al–Co and Al–Pt phase diagrams have been extensively studied (see updates in Refs. [1, 2] and [3, 4], respectively), the ternary Al–Co–Pt alloy system was investigated in the present contribution for the first time. This work continues the systematic

• E-mail address: b.grushko@fz-juelich.de

studies of the ternary alloy systems of Al–Pt with the transition elements (TM) of the VII and VIII groups of the periodic table: Al–Mn–Pt [5, 6], Al–Fe–Pt [7], Al–Ni–Pt [8], Al–Ru–Pt [9], Al–Rh–Pt [10], Al–Ir–Pt [11].

In the present work, the phase equilibria in the Al-rich part of Al–Co–Pt are studied at 1100 °C below 35 at.% Pt, at 850 °C below 25 at.% Pt and at 700 °C above 75 at.% Al. For the characterization of the phases revealed in the present study the results from Refs. [5-17] on the alloy systems of Al with the transition metals neighboring to Co and Pt were used.

2. Experimental

Master alloys of ~2 g were produced by levitation induction melting in a water-cooled copper crucible under a pure Ar atmosphere. The purity of Al was 99.999%, of Co 99.99%, of Pt 99.9%. Additional alloys of intermediate compositions were also produced by levitation induction melting from mixtures of the residuals of the previously studied ternary and binary samples.

The samples were annealed at 1100 °C under an Ar atmosphere (99.999% purity) or at 700 and 850 °C under vacuum of typically $9x10^{-7}$ mbar. The annealing times were 140 to 171 h at 1100 °C, 311 to 431 h at 850 °C, and 260 h at 700 °C. After annealing, the samples were quenched in water. The as-cast and annealed samples were examined by powder X-ray diffraction (XRD) and scanning electron microscopy (SEM). The compositions of the phases were measured by energy-dispersive X-ray analysis (EDX) in SEM on polished unetched surfaces (JEOL 840a scanning electron microscope equipped with EDAX Genesis 200 emission spectroscopy system). Powder XRD examinations were carried out using Cu Kα1 radiation and an imaging plate (Huber G670). The STOE software package was used for the indexing of the diffraction patterns and refinement of lattice parameters.

3. Results and discussion

3.1. Binary phases and their ternary extensions

The Al-rich regions of the binary Al–Co phase diagram (Fig. 1a) and Al–Pt phase diagram (Fig. 1b) are accepted according to Refs. [1, 2] and Refs. [3, 4], respectively. The crystallographic data of the relevant phases are included in Table 1.

The Al–Co phase diagram is naturally separated by the congruent equiatomic β_{Co}-phase on the Al-rich and Co-rich regions. No intermediate phases were revealed in the Co-rich region. In the Al-rich region there are Al_9Co_2 (θ_{Co}-phase), a bundle of the closely related $Al_{13}Co_4$ phases, and the Al_5Co_2 phase (H_{Co}-phase) [1, 2]. The Al-rich intermediate phases are coupled by a cascade of peritectic reactions which is ended by the (Al)-θ_{Co} eutectic.

The above-mentioned $Al_{13}Co_4$ bundle, forming in the compositional range of 23.5-25.5 at. % Co, includes stable O-$Al_{13}Co_4$, O′-$Al_{13}Co_4$, M-$Al_{13}Co_4$, m-$Al_{13}Co_4$ and the so-called Z-phase. The O′-$Al_{13}Co_4$ and O-$Al_{13}Co_4$ phases were observed at the stoichiometric composition at 1050 and 850 °C, respectively, while the others are somewhat depleted by Al. Apart from this, the formation of metastable o-$Al_{13}Co_4$ was reported in this compositional region. The detailed description of the complex $Al_{13}Co_4$ phase bundle still evokes the interest of researchers (see Ref. [18], for example).

The maximal ternary extension of the θ_{Co}-phase achieved ~4 at.% Pt, of m-$Al_{13}Co_4$ and H_{Co} ~2 and ~1.5 at.% Pt, respectively, all of them at constant Pt. The Al–Co Z-phase, O-$Al_{13}Co_4$ and M-$Al_{13}Co_4$ were not observed at ternary compositions.

The Al–Pt phase diagram contains at the equiatomic composition the congruent high-temperature β_{Pt}-phase of the CsCl type structure. It is stable between 1554 and 1260 °C (at slightly lower Al), while the low-temperature equiatomic μ_{Pt}-phase is formed below 1468 °C. In the Al-rich region of Al–Pt, there are the phases λ_{Pt} (Al_4Pt), high-temperature ξ_{Pt} ("Al_3Pt"), γ_{Pt} ($Al_{21}Pt_8$), β^* (Al_2Pt) and δ_{Pt} (Al_3Pt_2). The formation of a metastable phase from the ε_i-family and the metastable χ-phase was argued [4]. Both these structures were revealed at ternary compositions (see below).

The λ_{Pt}-phase was found to extend up to ~8 at.% Co at a practically constant Al concentration, but only up to ~3.5 at.% Co was revealed in the ξ_{Pt}-phase. Thus, the powder XRD patterns of an $Al_{76}Co_4Pt_{20}$ alloy annealed at 850 °C and containing the major ξ_{Pt}-phase (Fig. 2a) was reliably indexed using its preliminary structural model, similarly to that already reported in Ref. [4] for the binary ξ_{Pt}-phase. The refined lattice parameters of the ξ_{Pt}-phase are included in Table 1. The theoretical powder XRD pattern calculated for these lattice parameters was in qualitative agreement with the experimental data (see Fig. 3a vs. 3b). In contrast to the ξ_{Pt}-phase, the Al

concentration of the β*-phase extended from Al_2Pt was found to decrease with the increasing Co concentration and its extension was observed up to at least $Al_{57}Co_{16}Pt_{27}$. The refined lattice parameters of the essentially ternary β*-phase are included in Table 1.

The continuity of the ternary region between isostructural β_{Co} and high-temperature β_{Pt} was not tested. Under the conditions of the present experiment, the ternary extension of β_{Co} was only observed up to ~5 at.% Pt.

3.2. Ternary phases and phase equilibria of Al–Co–Pt

Four ternary phases, designated χ, ε, æ and D, were revealed in the temperature range of 700 to 1100 °C.

The structure of a phase forming between ~$Al_{76.5}Co_{11}Pt_{12.5}$ and $Al_{75}Co_4Pt_{21}$ was found to resemble that of $Al_{28}Ir_9$ (χ-phase) [12]. For example, a powder XRD pattern of this major phase is shown in Fig. 2b. It was reliably indexed using the structural model of $Al_{28}Ir_9$ from Ref. [12], where the Co and Pt atoms were suggested to occupy the positions of Ir. The refined lattice parameters of the ternary Al–Co–Pt χ-phase are included in Table 1. The theoretical powder XRD pattern calculated for these lattice parameters was in good agreement with the experimental data (see Fig. 3c vs. 3 d). This allows us to conclude that also Co stabilizes the above-mentioned metastable Al–Pt χ-phase, in addition to Mn, Fe, Ni, Ru or Rh (see more below).

The other compound forming between ~$Al_{75}Co_{17}Pt_8$ and $Al_{72}Co_7Pt_{21}$ was identified with a phase belonging to the so-called ε_i-family. The corresponding powder XRD pattern is shown in Fig. 2c. It was reliably indexed using the structural model of Ref. [13] for the Al–Pd–(Mn) ε_6-phase (designated ξ′ in [13]), where it was suggested that the Pt and Co atoms were occupying the positions of Pd and Mn, respectively. Thus, the theoretical powder XRD pattern calculated for the refined lattice parameters was in fair agreement with the experimental data (see Fig. 3e vs. 3f). The same was performed for the two other compositions from the above-mentioned wide range. The refined lattice parameters of the ternary Al–Co–Pt ε_6-phases are included in Table 1.

An additional æ-phase with a complex powder XRD pattern was revealed around ~$Al_{71}Co_{20}Pt_9$. No single æ-phase was produced; the powder XRD pattern of $Al_{70}Co_{19}Pt_{11}$ in Fig. 2d contained the lines of this major phase together with those of β* and β_{Co} (for comparison see Fig. 2e, which only exhibits the lines of β* and β_{Co} of the corresponding compositions). The equivalent

composition of the æ-phase is quite close to the compositional region of Al–Co–Pd where the ternary phases V, F and U are formed (see Ref. [14]) but was not identified with either of them.

The structure forming around the $Al_{73.4}Co_{23.3}Pt_{3.3}$ compositions was concluded to be decagonal (D-phase). Its typical powder XRD was revealed in an as-cast $Al_{72.5}Co_{22.5}Pt_5$ alloy containing this major phase (Fig. 4a), which survived annealing at 1100 °C for 142 h. After the annealing the fraction of this phase was significantly smaller and the corresponding powder XRD pattern contained the strong reflections of the neighboring æ-phase (see Fig. 4b). Since no single D-phase was produced in annealed samples, for its identification two relevant powder XRD patterns were subtracted. The resulting diffraction pattern in Fig. 4c was indeed typical of the decagonal phase with the periodicity of ~0.8 nm in the specific direction (D_2-phase, compare to Fig. 4d reproduced from Fig. 8c of Ref. [16] and to Figs. 2a,c of Ref. [15]).

Basing on the study of a series of samples thermally annealed at 1100, 850 and 700 °C, the corresponding partial isothermal sections of Al–Co–Pt were constructed (see Fig. 5). The three-phase equilibria marked by broken lines were estimated based on the experimental data of the neighboring regions. The highest applied temperature of 1100 °C is above the melting temperatures of the Al-rich binary phases θ_{Co}, O′-$Al_{13}Co_4$, M-$Al_{13}Co_4$, λ_{Pt}, and ξ_{Pt}. The β*-phase strongly propagates into the ternary region. At 1100 °C (Fig. 5a) it was found in equilibrium with β_{Co} and the ternary phases æ and ε. This isothermal section contains all four revealed ternary phases.

The narrow H+D and m+D two-phase regions are shown provisionally. Although inside the region bounded by the H, Z, m and D phases no experimental data were obtained at 1100 °C, only either H-m or Z-D two-phase equilibria are possible according to the phase rule. The former was confirmed at 850 °C (see Fig. 5b) which is in favor of the choice presented in Fig. 5a. This shrinks a possible propagation of the D-phase region towards the binary Al–Co terminal where the D-phase is already unstable. The binary peritectic temperature of the Z-phase formation (see Fig. 1a) is only ~50 °C above that of the 1100 °C isothermal section which leaves little room for the D-phase region.

The 850 °C isothermal section (Fig. 5b) includes the ternary extensions of the θ-Al_9Co_2 and ξ_{Pt}-phases. The binary O/O′-$Al_{13}Co_4$, M-$Al_{13}Co_4$ phases and Z-phase, stable at this temperature, were not observed at ternary compositions due to low solubility of Pt in these structures. On the other hand, the high-temperature m-$Al_{13}Co_4$ phase is not stable at its binary composition, but was

observed at ternary compositions due to its stabilization by Pt. The boundaries of the æ-β*-ε and æ-β-β* compositional triangles are close to those at 1100 °C. The coexistence of the H_{Co}-phase with the ε-phase at 850 °C instead of the D-æ equilibrium at 1100 °C is in favor of the high-temperature nature of the D-phase.

Three samples studied at 700 °C allowed the θ_{Co}-λ_{Pt}-L, θ_{Co}-m_{Co}-ε and λ_{Pt}-β* equilibria to be established (Fig. 5c).

3.3. Comparison to other Al–TM alloy systems

The Al concentration of the β*-phase, propagating from Al_2Pt, sharply decreases with the increasing Co concentration. This is in contrast to the compositional ranges of the other phases in the Al–Co–Pt alloy system either extending along constant Al or with slightly decreasing Al concentration with the decreasing Co concentration. Such a behavior of β* was also revealed in other ternary alloy systems based on Al–Pt (see Refs. [5, 7, 8], for example). Indeed, this phase is built from the 8 unit cells of the equiatomic β-phase (cP2 structure) with 4 vacant central atoms, which results in the cF12-type structure and composition Al_2Pt. In Al–Pt–TM alloys, these vacant positions are filled by the atoms of the third (TM) elements. Thus, in Al–Pt–Ni the β*-phase extends up to Al_2PtNi as is shown in Fig. 6 (β^{*Ni} in the following, the superscripts are added to discriminate the TMs dissolving in β*). At Al_2PtNi and around this composition, β^{*Ni} has already the Heusler-type structure (cF16) [8], while closer to the binary terminals the cP2-structure remains (see Fig. 6). On the other hand, a continuity between the isostructural Al–Fe and Al–Pt β-phases was concluded to be rather implausible at any temperature. Instead, the compositional region of the β^{*Fe}-phase propagates below 50 at. % Al at an almost constant Pt concentration [7]. The β^{*Mn}-phase region already extended up to the $Al_{20.0}Mn_{52.4}Pt_{27.6}$ composition [5]. In the Al–Co–Pt alloy system the propagations of the compositional region of β_{Co} and β* were only studied within the limits shown in Fig. 5. It can be seen in Fig. 6 that the slope of the compositional region of β^{*Co} is intermediate between those of β^{*Fe} and β^{*Ni}. In contrast to the above-mentioned, the propagation of the β^{*Ir}-phase [11] is very limited and occurs with only a slight decrease of the Al concentration with increasing Ir concentration (see Fig. 6).

The ternary χ-phase revealed in Al–Co–Pt is also typical of other Al–TM–Pt systems (TM = Mn, Fe, Ni, Ru, Rh, see Refs. [5-10] and references therein). In all these systems the third elements

stabilize the above-mentioned metastable Al–Pt χ-phase, while in Al–Ir–Pt its compositional region propagates from Al–Ir up to almost Al–Pt terminal [11]. The compositional regions of the χ-phases in selected alloy systems are compared in Fig. 7a.

The other above-mentioned metastable Al–Pt phase, ε-phase, is stabilized, apart from Co, also by Fe [7] or Ni [8]. The corresponding overall compositional regions of these ternaries are included in Fig. 7b. Being metastable in Al–Pt, the ε-phase is well known as a stable phase in Al–Pd, where two structural variants designated ε_6 and ε_{28} were revealed (see Ref. [14] and references therein). In Al–Co–Pd the ternary ε-region extends from Al–Pd up to ~15 at.% Co, and additional structural variants were revealed at ternary compositions by electron diffraction [14]. The majority of the equivalent compositions of the Al–Co–Pt ε-phase overlap with the Co-rich part of the ternary extension of the ε-phase in Al–Co–Pd (Fig. 7b). The present, only powder XRD, examinations do not allow verifying the existence of the structural variants of ε others than ε_6.

The compositional region of the Al–Co–Pt D-phase revealed in the present study is compared in Fig. 7c to those in Al–Co–Ni(Cu) [15] and Al–Co–Ir [16]. As was reported in Ref. [15] and references therein, several structural variants of the D-phase are typical of different compositions inside the continuous Al–Co–Cu and Al–Co–Ni regions depicted in Fig. 7c. In the Co-rich subregions colorized in Fig. 7c, the D-phase with the periodicity of ~0.8 nm in the specific direction (D_2-phase) was revealed. The extrapolations of the compositional regions of these phases towards the binary Al–Co terminal (broken lines in Fig. 7c) lead to a composition of ~$Al_{73}Co_{27}$. An essentially single D_2-phase of this composition was produced from the melt of ~Al_3Co under the conditions of strong undercooling [17] and conserved down to room temperature. However, by subsequent annealing it was destroyed with the formation of the stable phases depicted in the phase diagram in Fig. 1a. As is shown in Fig. 7c, the stabilization of the metastable Al–Co decagonal phase requires even less Pt than Cu or Ni. In contrast to that known presently in Al–Co–Ni(Cu), the Al–Co–Pt D-phase is only stable at elevated temperatures. On the other hand, no stabilization of the Al–Co D-phase was observed in Al–Co–Pd [14] and Al–Co–Rh [16].

Summary

- Partial 1100, 850 and 700 °C isothermal sections of Al–Co–Pt were constructed.
- The ternary extensions of θ-Al_9Co_2, m-$Al_{13}Co_4$ and H-Al_5Co_2 achieve ~4, ~2 and 1.5 at.% Pt, respectively.
- The ternary extensions of λ-Al_4Pt and ξ_{Pt} achieve ~8 and 3.5 at.% Co, respectively.
- The ternary extension of β*-Al_2Pt was found to propagate up to at least $Al_{57}Co_{16}Pt_{27}$.
- The formation of four ternary phases, designated χ, ε, æ, and D was revealed.
- The χ-phase (*P*31*c*, *a* = 1.21617 nm, *c* = 2.7115 nm) was revealed between ~$Al_{76.5}Co_{11}Pt_{12.5}$ and $Al_{75}Co_4Pt_{21}$.
- The ε-phase (ε_6-type, *Pnma, a* = 2.3116 nm, *b* = 1.6363 nm, *c* = 1.2150 nm) was revealed between ~$Al_{75}Co_{17}Pt_8$ and $Al_{72}Co_7Pt_{21}$.
- The D-phase of the D_2-type is formed at elevated temperatures in a small compositional region around $Al_{73.4}Co_{23.3}Pt_{3.3}$.
- The structure of the æ-phase forming around ~$Al_{71}Co_{20}Pt_9$ was not specified.

Acknowledgements

The author thanks C. Thomas for technical contributions.

References

[1] B. Grushko, G. Cacciamani, Al–Co (Aluminium-Cobalt). In MSIT workplace (online https://www.msiport.com/msit/msit). G. Effenberg (Ed.), MSI, Stuttgart.

[2] B. Grushko, W. Kowalski, S. Mi, J. Alloys Comp. 739 (2018) 280.

[3] A.J. McAlister, D.J. Kahan, Bull. Alloy Phase Diagrams 7 (1986) 47.

[4] B. Grushko, D. Kapush, J. Su, W. Wan, S. Hovmöller, J. Alloys Comp. 580 (2013) 618.

[5] B. Grushko, J. Alloys Comp. 792 (2019) 1223.

[6] S. Syniakina, B. Grushko, L. Meshi, J. Alloys Comp. 792 (2023) 171260.

[7] B. Grushko, J. Alloys Comp. 829 (2020) 154444.

[8] B. Grushko, D. Kapush, J Alloys Comp. 594 (2014) 127.

[9] D. Kapush, S. Samuha, L. Meshi, T.Ya. Velikanova, B. Grushko, Phase Equlibr. Diffus. 36 (2015) 327.

[10] B. Grushko, J. Alloys Comp. 636 (2019) 329.

[11] B. Grushko, S. Samuha, L. Meshi, J. Alloys Comp. 646 (2015) 873.

[12] S. Katrych, V. Gramlich, W. Steurer, J. Alloys Comp. 407 (2006) 132.

[13] M. Boudard, H. Klein, M. de Boissieu, M. Audier, Phil. Mag. A74 (1996) 939.

[14] a) M. Yurechko, B. Grushko, T. Velikanova, K. Urban, J. Alloys Comp. 337 (2002) 172.
b) I. Černičková, L. Ďuriška, P. Švec, P. Švec Sr., M. Mihalkovič, P. Priputen, P. Šulhánek, J. Janovec, J. Alloys Comp. 896 (2021) 162898.

[15] B. Grushko, K. Urban, Phil. Mag. B, 70 (1994) 1063.

[16] B. Grushko, J. Alloys Comp. 772 (2019) 399.

[17] J. Schroers, D. Holland-Moritz, D.M. Herlach, B. Grushko, K. Urban, Mater. Sci. Eng. A226-228 (1997). 990.

[18] P. Simon, I. Zelenina, R. Ramlau, W. Carrillo-Cabrera, U. Burkhardt, H. Borrmann, R. Cardoso Gil, M. Feuerbacher, P. Gille, Y. Grin, J. Alloys Comp. 820 (2020) 153363.

Figure captions

Fig. 1. Al-rich regions of the binary phase diagrams of: a) Al−Co according to Refs. [1, 2], b) Al−Pt according to Refs. [3, 4]. The provisional broken line in (a) separates the regions of L–O′-$Al_{13}Co_4$ (above) and L–O-$Al_{13}Co_4$ (below).

Fig. 2. Powder XRD patterns (Cu Kα1 radiation) of the: a) $Al_{77}Co_{3.5}Pt_{19.5}$ alloy annealed at 850 °C for 431 h and containing the essentially single ξ_{Pt}-phase, b) $Al_{77}Co_{3.5}Pt_{19.5}$ alloy annealed at 1100 °C for 142 h and containing the major χ-phase, c) $Al_{74}Co_{13}Pt_{13}$ alloy annealed at 1100 °C for 171 h and containing the single ε_6-phase, d) $Al_{70}Co_{19}Pt_{11}$ alloy annealed at 1100 °C for 142 h and containing the major æ-phase and minor β* and β_{Co}, e) $Al_{57}Co_{19}Pt_{24}$ alloy annealed at 1100 °C for 171 h and containing the major β*-phase and minor β_{Co}-phase (marked by arrows).

Fig. 3. Selected representative ranges of the experimental powder XRD patterns (Cu Kα1 radiation) of: ξ_{Pt} (a), χ (c) and ε (e), compared to the XRD patterns calculated according to the corresponding structural models of: Ref. [4] (b), Ref. [12] (d) and Ref. [13] (e), respectively (in color in the web version).

Fig. 4. Powder XRD patterns (Cu Kα1 radiation) of the D-phase: a) in the as-cast $Al_{73}Co_{22}Pt_5$ alloy, b) in the same alloy annealed at 1100 °C for 142 h, c) as in (b) after subtraction of the powder XRD pattern of the $Al_{70}Co_{25}Pt_5$ alloy annealed at 1100 °C for 171 h. For comparison, in Fig. 4d the powder XRD pattern of the $Al_{71.4}Co_{22.6}Ir_6$ D-phase is reproduced from Fig. 8c of Ref. [16]. (in color in the web version).

Fig. 5. Partial isothermal sections of Al−Co−Pt at: a) 1100 °C, b) 850 °C and c) 700 °C. L is the liquid. Provisional lines are shown broken. Measured compositions of the phases are marked by open squares and of the alloys by closed squares.

Fig. 6. Comparison of the ternary compositional regions of the β*-phases forming in the Al−TM−Pt alloy systems. TM = Ni, Co, Fe, Mn, Ir and the compositional regions are designated as β^{*Ni} [8], β^{*Co} (this work), β^{*Fe} [7], β^{*Mn} [5], β^{*Ir} [11], respectively with the corresponding references. The compositional region of the Al−Ni−Pt $\beta_{Pt\text{-}Ni}$ phase is extrapolated to higher temperatures basing on the data in Ref. [8]. (in color in the web version).

Fig. 7. Comparison of the compositional regions of the ternary: a) χ-phases in Al−TM−Pt (TMs marked in the figure are Ir [11], Rh [10], Ni [8], Mn [5], Co); ε-phases in Al−TM−Pt (TMs marked in the figure are Ni [8], Fe [7], Co) and in Al−Co−Pd [14]; c) D-phases in Al−Co−TM (TMs marked in the figure are Cu [15], Ni [15], Ir [16], Pt). In the Co-rich subregions colorized in (c), the D-phase with the periodicity of ~0.8 nm in the specific direction (D_2-phase) was revealed. The extrapolations of these compositional regions towards the binary Al–Co terminal marked by broken lines led to a composition of ~$Al_{73}Co_{27}$. (in color in the web version).

Table 1. Phases mentioned in the text and diagrams. TW – this work.

Phase	Space group or symmetry	Lattice parameters			Ref. Comment
		a, nm	*b*, nm	*c*, nm	
		α, °	*β*, °	*γ*, °	
θ-Al_9Co_2	*P*2$_1$/*c*	0.62163	0.62883	0.85587	[1]
			94.772		
		0.62527(6)	0.63068(6)	0.8598(1)	TW, $Al_{81.8}Co_{14.2}Pt_{4.0}$
			94.885(7)		
O-$Al_{13}Co_4$	*Pmn*2$_1$	0.8158	1.2347	1.4452	[1]
O′-$Al_{13}Co_4$	*Pnma*	2.8894	0.8143	1.2356	[2]
M-$Al_{13}Co_4$	*C*2/*m*	1.5173	0.8109	1.2349	[1]
		-	107.84	-	
m-$Al_{13}Co_4$	*C*2/*m*	1.6989	0.4098	0.7478	[1]
		-	115.812	-	
Z	*C-center monocl.*	3.984	0.8148	3.223	[1]
		-	107.97	-	
H-Al_5Co_2	*P*6$_3$/*mmc*	0.7672	--	0.7605	[1]
β_{Co}	$Pm\bar{3}m$	0.2862	--	--	for $Al_{50}Co_{50}$ [1]
λ_{Pt}-Al_4Pt	*P*3c1	1.3089	-	0.9633	[4]
		1.2971(6)	-	0.9678(2)	TW, $Al_{80.0}Co_{8.0}Pt_{12.0}$
ξ_{Pt}	*Bmmb*	1.9718	1.6228	1.4266	[4]
		1.9680(2)	1.6194(2)	1.4196(1)	TW, $Al_{75.5}Co_{3.5}Pt_{21.0}$
γ-$Al_{21}Pt_8$	*I*4$_1$/*a*	1.2942	-	1.0659	[4]
β*-Al_2Pt	$Fm\bar{3}m$	0.59194	-	-	[4]
		0.59148(8)	-	-	TW, $Al_{64.0}Co_{4.0}Pt_{32.0}$
		0.58669(8)	-	-	TW, $Al_{58.7}Co_{13}Pt_{28.3}$
χ	*P*31c [b]	1.21617(7)	-	2.7115(1)	TW, $Al_{75.0}Co_{4.0}Pt_{21.0}$
		1.2136(1)		2.7065(2)	TW, $Al_{76.0}Co_{9.0}Pt_{15.0}$
ε (ε$_6$)	*Pnma*	2.3116(3)	1.6363(2)	1.2150(1)	TW, $Al_{74.0}Co_{12.5}Pt_{13.5}$
		2.3120(5)	1.6314(5)	1.2082(4)	TW, $Al_{73.0}Co_{17.0}Pt_{10.0}$
		2.3189(4)	1.6469(2)	1.2193(2)	TW, $Al_{72.0}Co_{7.0}Pt_{21.0}$
æ	?	**?**	**?**	**?**	TW, ~$Al_{71}Co_{20}Pt_9$
D	Decagonal				TW, $Al_{73.4}Co_{23.3}Pt_{3.3}$

[a] by analogy with the space group of the χ-phase of $Al_{28}Ir_9$ [12].

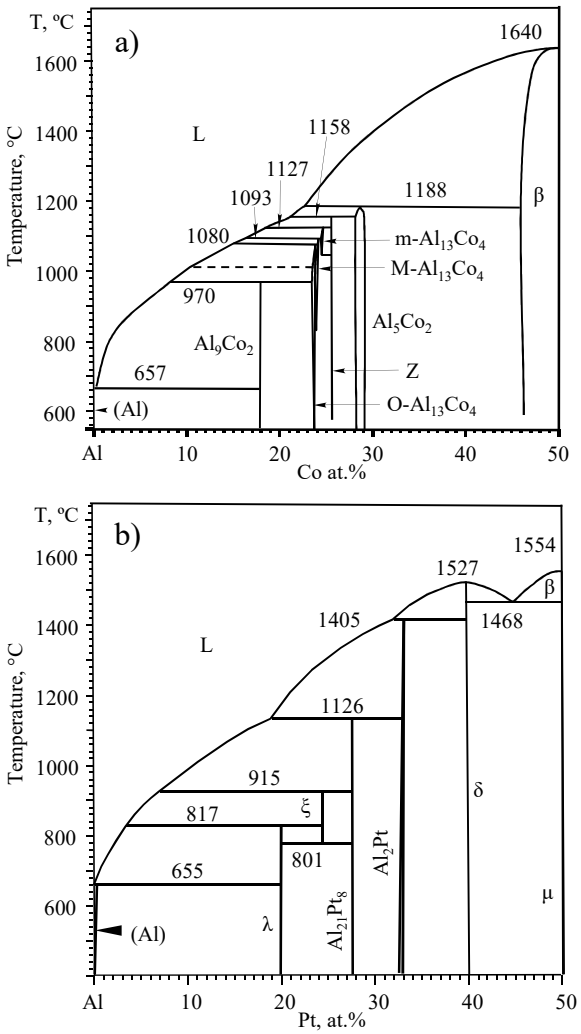
a)
T, ºC
Temperature, °C
1600
1400
1200
1000
800
600
L
1640
1158
1127
1093
1188
β
1080
m-Al13Co4
M-Al13Co4
970
Al5Co2
Al9Co2
657
Z
(Al)
O-Al13Co4
Al
10
20
30
40
50
Co at.%
b)
T, ºC
Temperature, °C
1600
1400
1200
1000
800
600
1554
1527
β
1405
1468
L
1126
915
δ
817
ξ
801
Al2Pt
655
λ
Al21Pt8
μ
(Al)
Al
10
20
30
40
50
Pt, at.%

Fig. 1

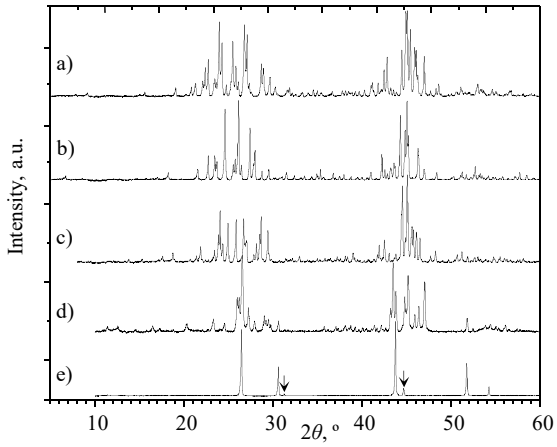

Fig. 2

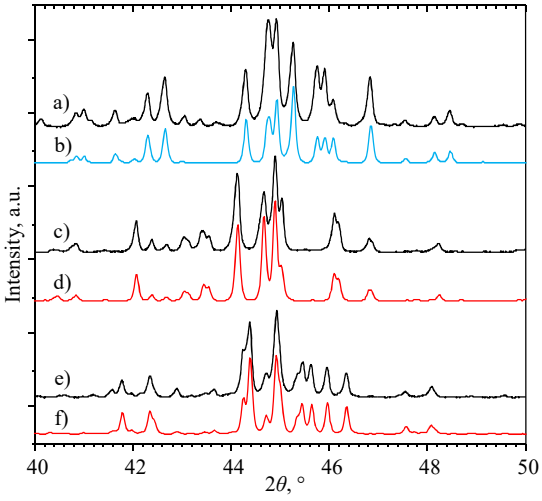

Fig. 3

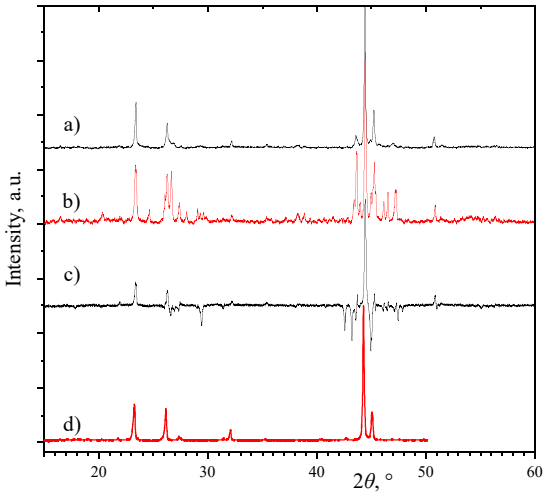

Fig. 4

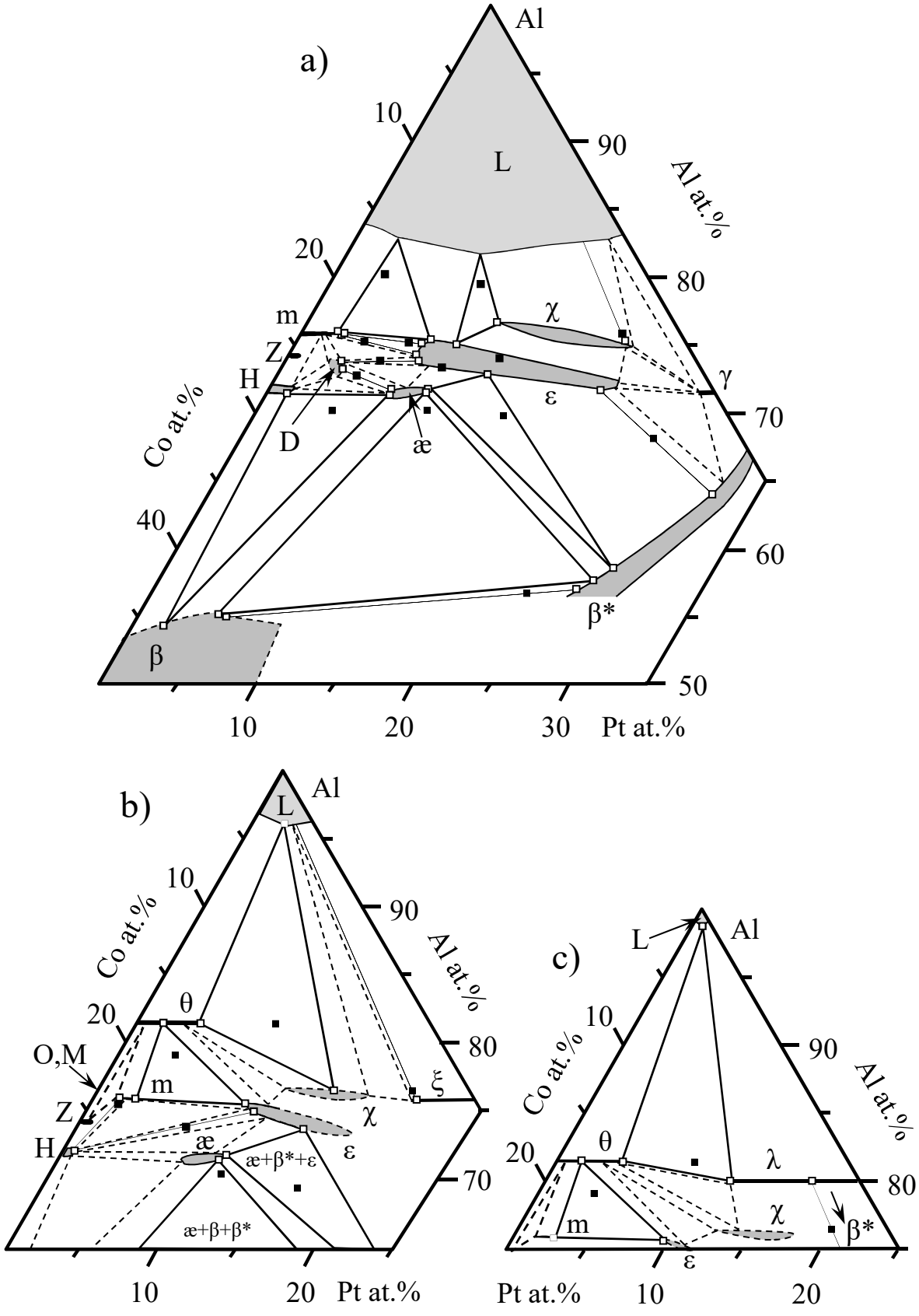
a)
Al
L
10
90
Al at.%
20
80
m
χ
Z
H
ε
γ
70
Co at.%
D
æ
40
60
β*
β
50
10
20
30
Pt at.%
b)
L
Al
10
Co at.%
90
Al at.%
θ
20
80
O,M
m
ξ
Z
χ
H
æ
ε
æ+β*+ε
70
æ+β+β*
10
20
Pt at.%
c)
L
Al
10
90
Co at.%
Al at.%
θ
20
λ
80
m
χ
β*
ε
Pt at.%
10
20

Fig. 5

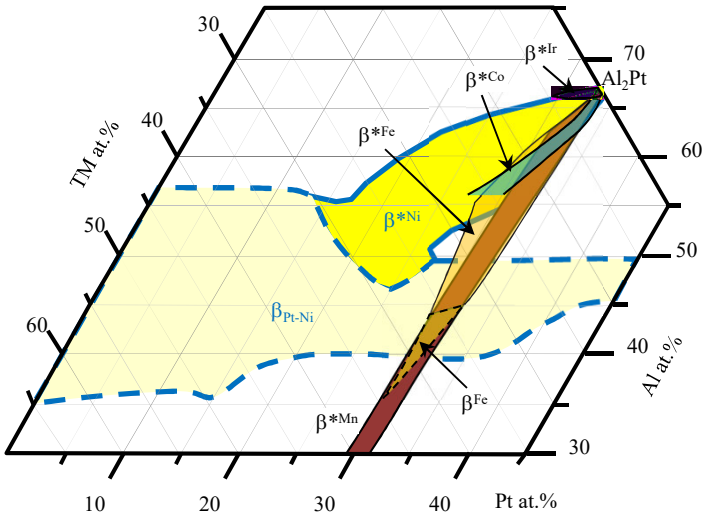
30
40
50
60
TM at.%
β*Ir
β*Co
β*Fe
β*Ni
β$_{Pt-Ni}$
β*Mn
β^{Fe}
70
Al$_2$Pt
60
50
40
30
Al at.%
10
20
30
40
Pt at.%

Fig. 6

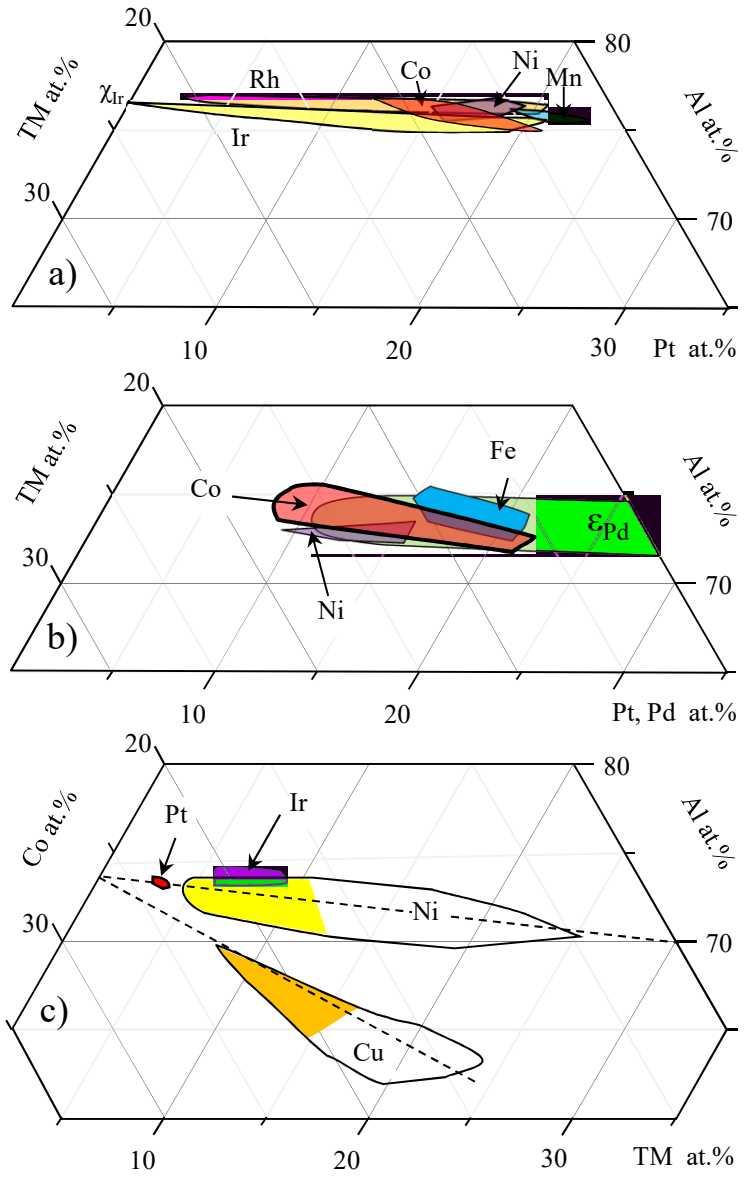
20
80
TM at.%
Al at.%
χIr
Rh
Co
Ni
Mn
Ir
30
70
a)
10
20
30
Pt at.%
20
TM at.%
Fe
Co
Al at.%
εPd
30
70
Ni
b)
10
20
Pt, Pd at.%
20
80
Co at.%
Al at.%
Pt
Ir
Ni
30
70
c)
Cu
10
20
30
TM at.%

Fig. 7